ISSN (Print) 1226-1750
ISSN (Online) 2233-6656
Journal of Magnetics 23(3), 409-415 (2018) https://doi.org/10.4283/JMAG.2018.23.3.409

Use of Vanadium Oxide as a Liquid Phase Sintering Aid for Barium Hexaferrite

John G. Fisher[1]*, Phan Gia Le[1], Hak-Sang Han[1], Su-Min Jeong[1], Naomi Karina Cabral de Leon[2] and Alejandro Danies Lopez[3]

[1]*School of Materials Science and Engineering, Chonnam National University, 77 Yongbong-ro, Buk-gu, Gwangju 61186, Republic of Korea*
[2]*Department of Industrial Engineering, Santo Domingo Institute of Technology, Avenida de Los Próceres #49, Los Jardines del Norte 10602, Santo Domingo, Dominican Republic*
[3]*Department of Biomedical Engineering, EIA University, km 2 + 200 Vía al Aeropuerto José María Córdova, Envigado, Colombia*

(Received 4 July 2018, Received in final form 12 September 2018, Accepted 13 September 2018)

The use of V_2O_5 as a liquid phase sintering aid for $BaFe_{12}O_{19}$ is studied. Three weight % of V_2O_5 is added to a $BaFe_{12}O_{19}$ powder, samples are sintered at temperatures between 900-1250 °C and the effects of sintering aid addition on densification, microstructure, phase purity and magnetic properties are examined. Compared to $BaFe_{12}O_{19}$ without sintering aid addition, addition of 3 wt % V_2O_5 leads to a moderate improvement in densification behavior. Samples with 3 wt % V_2O_5 addition contain considerable amounts of Fe_2O_3 and $Ba_3(VO_4)_2$ second phases. The $BaFe_{12}O_{19}$ sample without sintering aid addition has a Magnetization-Field hysteresis loop typical of a hard ferrimagnetic material, whereas the 97 wt % $BaFe_{12}O_{19}$ - 3 wt % V_2O_5 sample has a hysteresis loop with reduced saturation magnetization and coercivity.

Keywords : ferrites, sintering, microstructure, magnetic properties

1. Introduction

Barium hexaferrite, $BaFe_{12}O_{19}$, is a hard ferrimagnetic material which finds many uses as permanent magnets, in recording media and in microwave applications [1-10]. For the preparation of bulk ceramics, $BaFe_{12}O_{19}$ is usually sintered at temperatures in the range 1100-1300 °C [11-13]. In order to reduce production costs and facilitate thick-film processing, it is often necessary to reduce the sintering temperature by addition of a liquid phase sintering aid. For low temperature co-fired ceramic applications, the sintering temperature should be lowered to 900 °C to allow the use of Ag electrodes [14, 15]. Several types of liquid phase sintering aid have previously been used to lower the sintering temperature of $BaFe_{12}O_{19}$ [12, 14-17]. CuO, $BaCuO_2$ and a BaO-CuO eutectic composition were used to reduce the sintering temperature to 1100 °C [12]. Use of a Bi_2O_3–B_2O_3–SiO_2–ZnO glass powder was effective in lowering the sintering temperature to 900 °C [15]. Use of Bi_2O_3 [14, 17] and Bi_2O_3 + CuO [17] could reduce the sintering temperature to within the range 920 °C-1020 °C. The addition of a liquid phase sintering aid may also cause abnormal grain growth even at lower sintering temperatures [12, 14].

During sintering, the liquid phase sintering aid melts to form a liquid which penetrates between the particles of the solid phase by capillary action. The liquid phase can then promote densification by the pore filling process [18]. To be successful, a liquid phase sintering aid should fulfil the following requirements: it should form a low temperature eutectic point with the solid phase, the solid phase should have a high solubility in the liquid, the liquid phase should have a low solubility in the solid, the liquid phase should wet the solid grains and the solid phase should have a high diffusion rate in the liquid phase [19].

The current work looks at the use of V_2O_5 as a liquid phase sintering aid for $BaFe_{12}O_{19}$. V_2O_5 has a melting point of 690 °C and has been used as a solid-state or liquid phase sintering aid for $(Zn_{1-x}Mg_x)TiO_3$ [20], Mg_2TiO_4 [21], $Zr_{0.8}Sn_{0.2}TiO_4$ [22], $LiNb_{0.6}Ti_{0.5}O_3$ [23], $SrBi_2Nb_2O_9$ [24], $(K_{0.5}Na_{0.5})NbO_3$ [25, 26] and $BiNbO_4$ [27]. The use of V_2O_5 was effective in lowering the sintering temperature of these materials. For example, the sintering temperature

©The Korean Magnetics Society. All rights reserved.
*Corresponding author: Tel: +82-62-530-1702
Fax: +82-62-530-1699, e-mail: johnfisher@jnu.ac.kr

© 2018 Journal of Magnetics

of $(Zn_{1-x}Mg_x)TiO_3$ ceramics could be reduced from 1200 °C to 875 °C by addition of 1 wt % V_2O_5 [20] and the addition of 0.5 wt % of V_2O_5 could lower the sintering temperature of Mg_2TiO_4 from 1400 °C to 1250 °C [21]. As far as we know, this compound has not been used as a liquid phase sintering aid for $BaFe_{12}O_{19}$. The low melting point of this compound may enable it to act as an effective liquid phase sintering aid for $BaFe_{12}O_{19}$. In addition to affecting the sintering behavior, addition of a liquid phase sintering aid may also affect the structure, microstructure and magnetic properties of $BaFe_{12}O_{19}$. This is also studied in the present work.

2. Experimental

A commercial $BaFe_{12}O_{19}$ powder (99.2 %, supplied by LG Innotek Co. Ltd.) was used. The powder was dried at 250 °C for 1 h to remove adsorbed water. To prepare the $BaFe_{12}O_{19}$ powder without sintering aid addition, 30 g of powder was weighed and then ball milled in high purity ethanol (99.9 %) with zirconia media in a polypropylene jar for 24 h. After evaporating the ethanol with a hot plate and stirrer, the powder was ground in an agate mortar and pestle and sieved to pass a 180 μm mesh. To prepare the powder with sintering aid addition, $BaFe_{12}O_{19}$ powder and V_2O_5 (99.6 %, Alfa Aesar) powder were dried at 250 °C for 1 h, weighed, ball milled, ground and sieved as above. The composition of the V_2O_5 - added powder is 97 wt % $BaFe_{12}O_{19}$ - 3 wt % V_2O_5.

Powders were pressed by hand in a stainless steel die of 10 mm diameter to form pellet-shaped samples. The samples were then cold isostatically pressed at a pressure of 147 MPa (1500 kgf). Samples were sintered in the temperature range 900-1250 °C for 1 h with heating and cooling rate of 5 °C·min^{-1}. To reduce Ba volatilization, samples were buried in $BaFe_{12}O_{19}$ packing powder in a double alumina crucible with lids.

The density of sintered samples was measured via the Archimedes principle in deionized water. The phase structure of selected samples was investigated by X-ray diffraction (XRD) with Cu K_α radiation (XRD XPert PRO, PANalytical, The Netherlands) with 2θ range = 20°-80°, scan speed = 3°.min^{-1} and 0.02° step size. Unit cell parameters were calculated from the XRD patterns by the least-squares method using the program Jade 6.5 (Materials Data Inc., CA). Samples were vertically sectioned using a low speed diamond wheel saw, polished to a 1 μm finish and thermally etched. Samples were Pt coated and the microstructure analyzed using scanning electron microscopy (SEM, Hitachi S-4700 FE-SEM, Hitachi High-Tech, Tokyo, Japan) with an attached energy dispersive spectrometer using standardless quantification (EDS, EMAX Energy EX-200, Horiba, Kyoto, Japan). The 2D equivalent mean grain size and standard deviation were measured from the SEM micrographs using ImageJ image analysis software (National Institute of Mental Health, Bethesda, MD). At least 150 grains were measured for each sample. Magnetization-magnetic field hysteresis loops were measured at room temperature using a vibrating sample magnetometer (VSM, Lake Shore VSM 704, Westerville, OH).

3. Results

The Archimedes density of the sintered samples is shown in Fig. 1. A theoretical density of 5.28 g·cm^{-3} for $BaFe_{12}O_{19}$ was used for all compositions. The density of the $BaFe_{12}O_{19}$ samples increases with sintering temperature, reaching a maximum value of 94.4 % theoretical density at 1250 °C. Addition of 3 wt % V_2O_5 has no effect on density at a sintering temperature of 900 °C and causes a moderate increase in the density of the sintered samples at sintering temperatures in the range 950-1100 °C. At higher temperatures, the increase in density tails off. The samples sintered at 1200 °C have a density almost the same as the $BaFe_{12}O_{19}$ samples and the samples sintered at 1250 °C have a noticeably lower density than that of the $BaFe_{12}O_{19}$ samples.

SEM micrographs of the $BaFe_{12}O_{19}$ samples without sintering aid addition sintered at temperatures between 900-1250 °C for 1 h are shown in Fig. 2. The mean equivalent spherical 2D grain size of all the samples is shown in Fig. 4. The error bars in Fig. 4 represent the standard deviation. The $BaFe_{12}O_{19}$ samples consist mainly of equiaxed matrix grains. The matrix grain size is initially

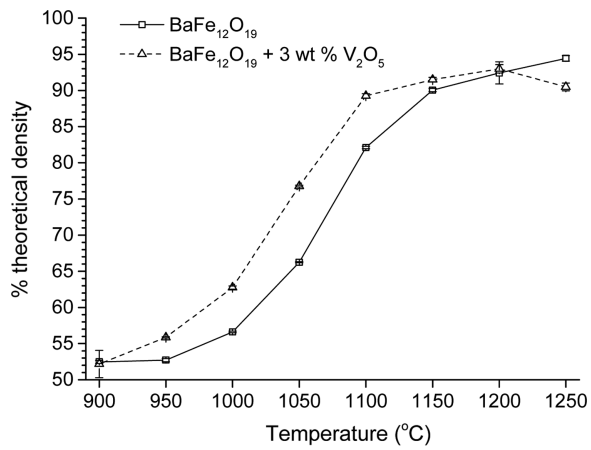

Fig. 1. Archimedes density of $BaFe_{12}O_{19}$ and 97 wt % $BaFe_{12}O_{19}$ – 3 wt % V_2O_5 samples sintered at 900-1250 °C for 1 h.

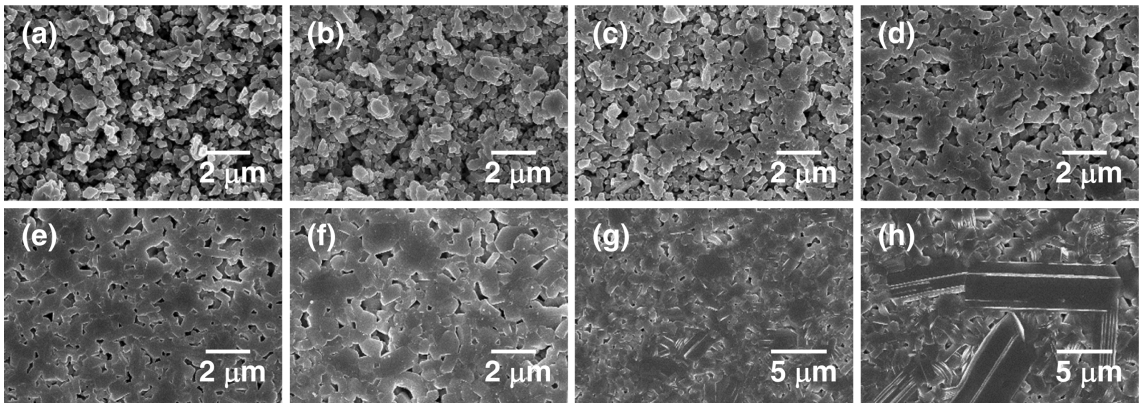

Fig. 2. SEM micrographs of $BaFe_{12}O_{19}$ samples sintered for 1 h at: (a) 900 °C; (b) 950 °C; (c) 1000 °C; (d) 1050 °C; (e) 1100 °C; (f) 1150 °C; (g) 1200 °C and (h) 1250 °C.

submicron and increases slightly with increasing sintering temperature, becoming micron-sized at 1200-1250 °C. Samples sintered at 950-1000 °C are still in the initial stage of sintering, with little formation of grain boundaries between the powder particles. Samples sintered between 1050 and 1150 °C are in the intermediate stage of sintering. Grain boundaries have formed between the particles but extensive interconnected pore channels still exist. Samples sintered at > 1150 °C are in the final stage of sintering, with isolated pores between the grains. The sample sintered at 1200 °C is in the initial stage of abnormal grain growth, with some grains ~3-5 μm in diameter. The sample sintered at 1250 °C contains abnormal grains up to 20 μm in diameter. The sample sintered at 1250 °C has some secondary phases present in the abnormal grains. A similar secondary phase was previously found in abnormal grains in $BaFe_{12}O_{19}$ and may be $BaFe_2O_4$ [28].

SEM micrographs of the 97 wt % $BaFe_{12}O_{19}$ - 3 wt % V_2O_5 samples sintered at temperatures between 900-1250 °C for 1 h are shown in Fig. 3. The microstructure of the samples in the range of 900-1050 °C is similar to that of the $BaFe_{12}O_{19}$ samples without sintering aid addition. Abnormal grains begin to appear in the sample sintered at 1100 °C. Abnormal grain growth becomes more prominent

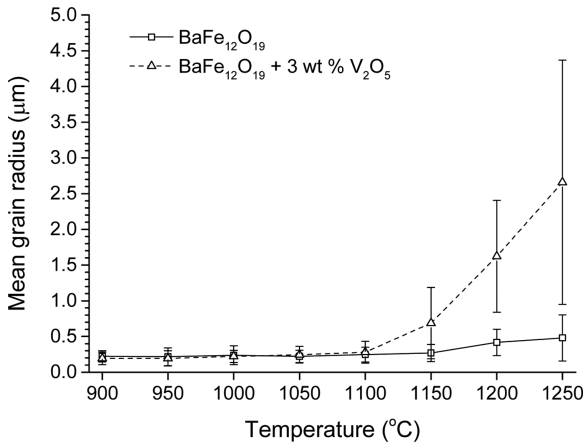

Fig. 4. Mean grain radius of $BaFe_{12}O_{19}$ and 97 wt % $BaFe_{12}O_{19}$ – 3 wt % V_2O_5 samples sintered at 900-1250 °C for 1 h.

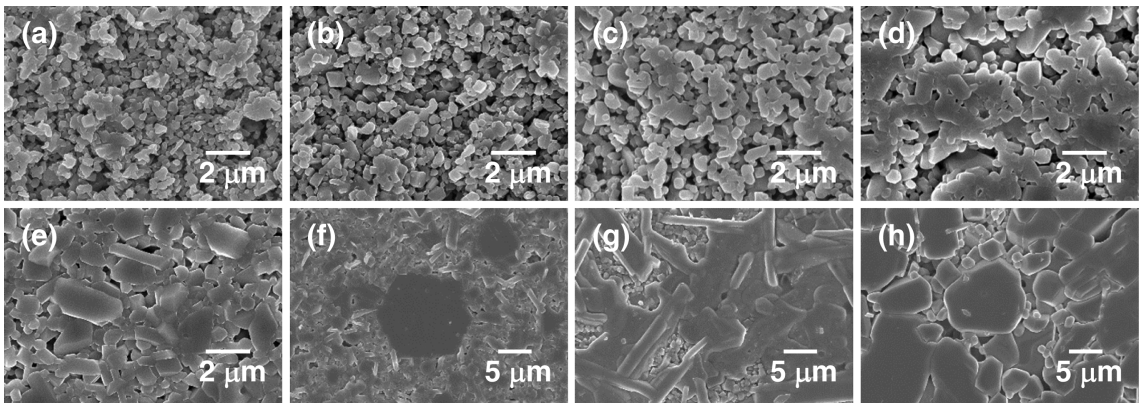

Fig. 3. SEM micrographs of 97 wt % $BaFe_{12}O_{19}$ – 3 wt % V_2O_5 samples sintered for 1 h at: (a) 900 °C; (b) 950 °C; (c) 1000 °C; (d) 1050 °C; (e) 1100 °C; (f) 1150 °C; (g) 1200 °C and (h) 1250 °C.

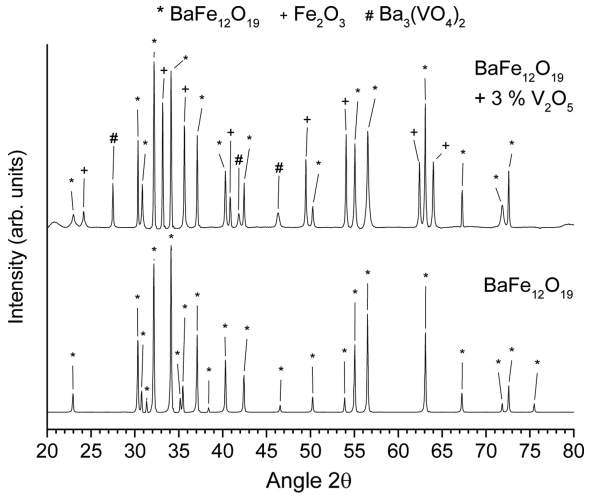

Fig. 5. XRD patterns of $BaFe_{12}O_{19}$ and 97 wt % $BaFe_{12}O_{19}$ – 3 wt % V_2O_5 samples sintered at 1250 °C for 1 h.

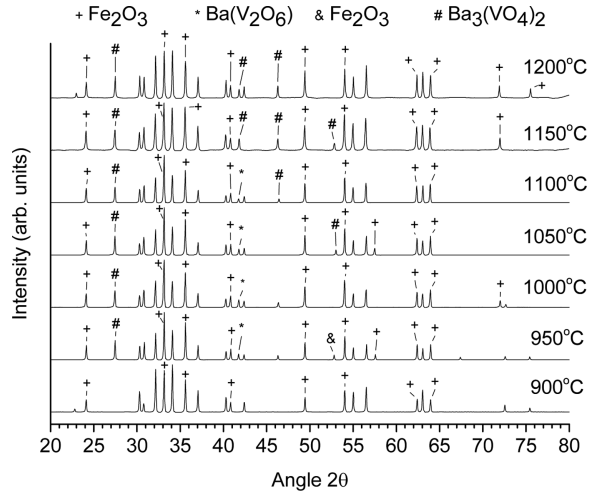

Fig. 6. XRD patterns of 97 wt % $BaFe_{12}O_{19}$ – 3 wt % V_2O_5 samples sintered in the temperature range 900-1200 °C for 1 h.

in the sample sintered at 1150 °C, with abnormal grains up to 10 μm in diameter present. This is reflected in the increase of the mean grain radius and the width of the error bars in Fig. 4. EDS analysis of the abnormal grains detects the presence of V (up to 2 at %) indicating that V_2O_5 has formed a solid solution with $BaFe_{12}O_{19}$. The number and size of the abnormal grains increases dramatically in the sample sintered at 1200 °C, with abnormal grains up to 50 μm in diameter present. There is also a plate-shaped secondary phase with increased V content (up to 11 at.%). The size of the abnormal grains in the sample sintered at 1250 °C decreases to a maximum of 10 μm. However, the number of abnormal grains increases, causing the mean grain radius to increase further.

XRD of the as-received $BaFe_{12}O_{19}$ powder shows it to consist of $BaFe_{12}O_{19}$ (ICDD card number 74-1121) with a secondary phase of α-Fe_2O_3 (ICDD card number 87-1166). XRD patterns of the $BaFe_{12}O_{19}$ and 97 wt % $BaFe_{12}O_{19}$ - 3 wt % V_2O_5 samples sintered at 1250 °C for 1 h are shown in Fig. 5. All the patterns can be indexed with ICDD card number 74-1121 for $BaFe_{12}O_{19}$. No peaks due to secondary phases are visible in the $BaFe_{12}O_{19}$ sample. The 97 wt % $BaFe_{12}O_{19}$ - 3 wt % V_2O_5 sample contains secondary phases of α-Fe_2O_3 (ICDD card number 87-1166) and $Ba_3(VO_4)_2$ (ICDD card number 71-2060). Unit cell parameters of the samples are shown in Table 1. The numbers in brackets show the error. The 97 wt % $BaFe_{12}O_{19}$ - 3 wt % V_2O_5 sample has a slightly larger *a* unit cell parameter and a slightly smaller *c* unit cell parameter than the $BaFe_{12}O_{19}$ sample.

XRD patterns of the 97 wt % $BaFe_{12}O_{19}$ - 3 wt % V_2O_5 samples sintered in the temperature range 900-1200 °C for 1 h are shown in Fig. 6. Again, all of the patterns can be indexed with ICDD card number 74-1121 for $BaFe_{12}O_{19}$ (the unmarked peaks). In all of the samples, peaks of an α-Fe_2O_3 secondary phase (ICDD card number 87-1166) are visible. In the sample sintered at 950 °C, a peak belonging to a different Fe_2O_3 second phase is present (ICDD card number 76-1821). In the samples sintered at ≥ 950 °C, peaks of a $Ba_3(VO_4)_2$ secondary phase (ICDD card number 71-2060) are visible. In the samples sintered in the range 950-1100 °C, peaks belonging to a $Ba(V_2O_6)$ secondary phase (ICDD card number 86-0240) are also present.

Magnetization-magnetic field (M-H) hysteresis loops of samples sintered at 1250 °C for 1 h are shown in Fig. 7. The magnetic properties are shown in Table 2. The M-H loops of the $BaFe_{12}O_{19}$ sample are typical of a hard ferrimagnetic material [3, 4]. The M-H loops of the 97 wt % $BaFe_{12}O_{19}$ - 3 wt % V_2O_5 sample are much slimmer with reduced coercivity, saturation magnetization and remanent magnetization. The similarity between the in-

Table 1. Unit cell parameters of samples sintered at 1250 °C for 1 hour.

Sample	*a* unit cell parameter (nm)	*c* unit cell parameter (nm)	Unit cell volume (nm^3)
$BaFe_{12}O_{19}$	0.588886(0.0000097)	2.32359(0.0000557)	0.69783
97 wt % $BaFe_{12}O_{19}$ - 3 wt % V_2O_5	0.589171(0.0001059)	2.320137(0.0008065)	0.69747

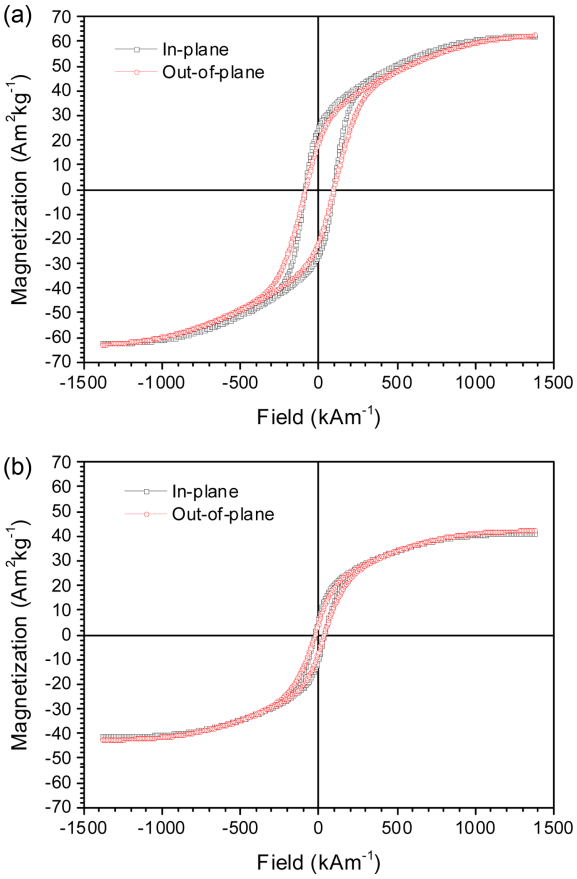

Fig. 7. (Color online) Magnetization vs. field hysteresis loops of (a) $BaFe_{12}O_{19}$ and (b) 97 wt % $BaFe_{12}O_{19}$ – 3 wt % V_2O_5 samples sintered at 1250 °C for 1 h.

plane and out-of-plane curves indicates that there is little preferred orientation of the grains in the samples.

4. Discussion

From the XRD patterns in Fig. 5 and Fig. 6 it is seen that V_2O_5 reacts considerably with $BaFe_{12}O_{19}$. V_2O_5 can react with $BaFe_{12}O_{19}$ as follows:

$$3\ BaFe_{12}O_{19} + V_2O_5 \rightarrow Ba_3(VO_4)_2 + 18\ Fe_2O_3 \quad (1)$$

$$BaFe_{12}O_{19} + V_2O_5 \rightarrow Ba(V_2O_6) + 6\ Fe_2O_3 \quad (2)$$

According to the BaO-V_2O_5 phase diagram of Kohlmuller and Perraud, $Ba_3(VO_4)_2$ melts incongruently at ~1100 °C and $Ba(V_2O_6)$ melts congruently at ~700 °C [29]. Therefore, the V_2O_5 may act as a transient liquid phase sintering aid, being consumed as it reacts with $BaFe_{12}O_{19}$. The $Ba(V_2O_6)$ phase would melt again, but the $Ba_3(VO_4)_2$ phase would remain solid. This would explain the limited improvement in densification of the 97 wt % $BaFe_{12}O_{19}$ - 3 wt % V_2O_5 samples between 950-1100 °C. The amount of liquid phase available to assist with densification would be less than expected due to the conversion of V_2O_5 into $Ba_3(VO_4)_2$. The detection of V in the abnormal grains by EDS and the changes in unit cell parameters (Table 1) also indicate that some of the V_2O_5 is forming a solid solution with $BaFe_{12}O_{19}$. The formation of more liquid phase at 1100 °C as the $Ba_3(VO_4)_2$ phase melts could promote abnormal grain growth in the 97 wt % $BaFe_{12}O_{19}$ - 3 wt % V_2O_5 samples sintered at ≥ 1100 °C (Fig. 3) [12]. Abnormal grain growth can be detrimental to densification by causing pores to be trapped inside the grains [30]. This may be the cause of the decrease in density at 1250°C. As the sintering temperature increases, the number of grains which can grow rapidly to form abnormal grains also increases [31]. Once the abnormal grains impinge upon each other, their growth rate decreases due to a reduction in their driving force for growth, which is inversely proportional to the grain size of the surrounding grains [28]. This explains why the abnormal grains in the 97 wt % $BaFe_{12}O_{19}$ - 3 wt % V_2O_5 sample sintered at 1250 °C are smaller than those of the sample sintered at 1200 °C. The larger number of abnormal grains in the sample sintered at 1250 °C leads to earlier impingement, limiting their growth.

Based on our previous work with CuO-based sintering aids [12] and on the results of other workers [14, 15], 3 wt % was chosen as the amount of V_2O_5 to add to $BaFe_{12}O_{19}$. This is larger than the amount of V_2O_5 added as a liquid phase sintering aid in previous works (usually 0.5-1.5 wt %) [20-22, 27]. Reducing the amount of V_2O_5 added to the $BaFe_{12}O_{19}$ would reduce the formation of secondary phases and may improve the sintering behavior. Adding $BaCO_3$ along with V_2O_5 may avoid the decomposition of $BaFe_{12}O_{19}$ as the $BaCO_3$ could react with the

Table 2. Magnetic properties of samples sintered at 1250 °C for 1 hour.

Sample	In-plane saturation magnetization M_s (Am^2kg^{-1})	In-plane remanent magnetization M_r (Am^2kg^{-1})	In-plane coercivity H_c (kAm^{-1})	Out-of-plane saturation magnetization M_s (Am^2kg^{-1})	Out-of-plane remanent magnetization M_r (Am^2kg^{-1})	Out-of-plane coercivity H_c (kAm^{-1})
$BaFe_{12}O_{19}$	56	26	95	61	20	93
97 wt % $BaFe_{12}O_{19}$ - 3 wt % V_2O_5	40	8	31	41	6	30

V_2O_5 to form $Ba(V_2O_6)$. Another possibility would be to use $Ba(V_2O_6)$ instead of V_2O_5, thereby avoiding the formation of secondary phases by reactions (1) and (2).

The reduction in coercivity of the 97 wt % $BaFe_{12}O_{19}$ - 3 wt % V_2O_5 sample (Fig. 7) is caused by the large grain size of the abnormal grains (Fig. 3). Each grain in the sample consists of a number of domains, in which the net magnetic moments of the unit cells align in the same direction [3]. The magnetization in the sample can change either by rotating the magnetization vectors in the domains in the direction of the external magnetic field or by the movement of magnetic domain walls. The domains with magnetization vectors pointing close to the direction of the magnetic field will grow at the expense of domains with magnetization vectors pointing away from the direction of the magnetic field [3]. The grain boundaries pin the magnetic domain walls, hindering their motion [11]. The larger grain size means less grain boundary area and therefore less pinning of the domain walls. Large grains also contain a larger number of domain walls than small grains, leading to a greater contribution of domain wall movement to the magnetization [30]. The reduction in saturation magnetization and remanent magnetization is due to the formation of α-Fe_2O_3 secondary phase, which is antiferromagnetic or weakly ferromagnetic [32].

The 12 Fe^{3+} ions in the $BaFe_{12}O_{19}$ formula unit are distributed over nine octahedral sites (co-ordination number CN = 6), two tetrahedral sites (CN = 4) and one trigonal bi-pyramidal site (CN = 5) [1, 3, 4]. Eight Fe^{3+} ions have spins in the up direction, and four Fe^{3+} ions have spins in the down direction, giving twenty unpaired spins (20 μ_B, where μ_B = Bohr magneton) per formula unit. From Shannon [33], the ionic radii of Fe^{3+} are 0.049 nm, (CN = 4), 0.058 nm (CN = 5), and 0.0645 nm (CN = 6). The ionic radii of V^{5+} are 0.0355 nm (CN = 4), 0.046 nm (CN = 5), and 0.054 nm (CN = 6). V may also change oxidation state e.g. to V^{3+} with an ionic radius of 0.064 nm (CN = 6). V^{5+} would be expected to replace Fe^{3+} ions in the $BaFe_{12}O_{19}$ crystal lattice due to their similar size. The changes in unit cell parameters and unit cell volume indicate that some substitution takes place (Table 1). V^{5+} would have no unpaired d-shell electrons and V^{3+} two unpaired d-shell electrons, so substitution for Fe^{3+} could also be expected to reduce the magnetic moment.

5. Conclusions

The use of V_2O_5 as a liquid phase sintering aid for $BaFe_{12}O_{19}$ is studied. Three wt % V_2O_5 addition leads to a moderate improvement in densification behavior. Samples with V_2O_5 addition contain considerable amounts of α-Fe_2O_3 and $Ba_3(VO_4)_2$ secondary phases. The $BaFe_{12}O_{19}$ sample has a Magnetization-Field hysteresis loop typical of a hard ferrimagnetic material, whereas the 97 wt % $BaFe_{12}O_{19}$ - 3 wt % V_2O_5 sample has a hysteresis loop with reduced saturation magnetization and coercivity. This is due to the decomposition of $BaFe_{12}O_{19}$ into $Ba_3(VO_4)_2$ and Fe_2O_3 and extensive abnormal grain growth. Based on these results, 3 wt % addition of V_2O_5 is not a suitable liquid phase sintering aid for $BaFe_{12}O_{19}$. Reducing the amount of V_2O_5 added may improve the sintering behaviour while reducing secondary phase formation.

Acknowledgements

This research was supported by the Basic Science Research Program through the National Research Foundation of Korea (NRF), funded by the Ministry of Education (grant number: 2015R1D1A1A01057060). The authors would like to thank Dr. Seok Bae (LG Innotek) for providing the $BaFe_{12}O_{19}$ powder, Kyeong-Kap Jeong (Center for Research Facilities, Chonnam National University) for operating the XRD, Hey-Jeong Kim for operating the SEM, and Prof. Byong-Guk Park (KAIST) for carrying out the VSM measurements.

References

[1] A. J. Moulson and J. M. Herbert, Electroceramics: Materials, Properties, Applications. 2nd Edition. John Wiley & Sons Ltd., Chichester (2003) pp 469-546.
[2] J. Jalli, Y. K. Hong, S. Bae, J. J. Lee, G. S. Abo, A. Lyle, S. H. Gee, H. Lee, T. Mewes, J. C. Sur, and S. I. Lee, J. Appl. Phys. **105**, 07A511 (2009).
[3] G. Alex, Modern Ferrite Technology. Springer, New York (2010) pp 51-70.
[4] R. C. Pullar, Prog. Mater. Sci. **57**, 1191 (2012).
[5] C. Gokulnath, S. Balaji, S. D. R. Prasath, S. Raju, and V. Abhaikumar, Materials Research Express **5**, 076103 (2018).
[6] D. A. Vinnik, D. A. Zherebtsov, L. S. Mashkovtseva, S. Nemrava, M. Bischoff, N. S. Perov, A. S. Semisalova, I. Krivtsov, L. I. Isaenko, G. G. Mikhailov, and R. Niewa, J. Alloys Compd. **615**, 1043 (2014).
[7] S. Jiao, M. Wu, X. Yu, H. Hu, Z. Bai, P. Dai, T. Jiang, H. Bi, and G. Li, Mater. Res. Bull. **108**, 89 (2018).
[8] D. S. Klygach, M. G. Vakhitov, D. A. Vinnik, A. V. Bezborodov, S. A. Gudkova, V. E. Zhivulin, D. A. Zherebtsov, C. P. SakthiDharan, S. V. Trukhanov, A. V. Trukhanov, and A. Y. Starikov, J. Magn. Magn. Mater. **465**, 290 (2018).
[9] J. Li, S. He, K. Shi, Y. Wu, H. Bai, Y. Hong, W. Wu, Q. Meng, D. Jia, and Z. Zhou, Ceram. Int. **44**, 6953 (2018).
[10] D. A. Vinnik, D. S. Klygach, V. E. Zhivulin, A. I.

Malkin, M. G. Vakhitov, S. A. Gudkova, D. M. Galimov, D. A. Zherebtsov, E. A. Trofimov, N. S. Knyazev, V. V. Atuchin, S. V. Trukhanov, and A. V. Trukhanov, J. Alloys Compd. **755**, 177 (2018).
[11] J. Dho, E. K. Lee, J. Y. Park, and N. H. Hur, J. Magn. Magn. Mater. **285**, 164 (2005).
[12] H. Vu, D. Nguyen, J. G. Fisher, W. H. Moon, S. Bae, H. G. Park, and B. G. Park, Journal of Asian Ceramic Societies **1**, 170 (2013).
[13] R. E. El Shater, E. H. El-Ghazzawy, and M. K. El-Nimr, J. Alloys Compd. **739**, 327 (2018).
[14] V. A. Rane, G. J. Phatak, and S. K. Date, IEEE Trans. Magn. **49**, 5048 (2013).
[15] Y. Wang, Y. L. Liu, J. Li, Q. Liu, H. W. Zhang, and V. G. Harris, AIP Adv. **6**, 056410 (2016).
[16] Y. Liu, Y. Li, H. Zhang, D. Chen, and Q. Wen, J. Appl. Phys. **107**, 09A507 (2010).
[17] C. Wu, Z. Yu, G. Wu, K. Sun, Y. Yang, X. Jiang, R. Guo, and Z. Lan, IEEE Trans. Magn. **51**, 1 (2015).
[18] S. J. L. Kang, Sintering: Densification, Grain Growth & Microstructure. Elsevier Butterworth Heinemann, Amsterdam (2005) pp 227-247.
[19] R. M. German, Sintering Theory and Practice. Wiley, New York (1996) pp 225-312.
[20] X. C. Liu, F. Gao, M. Zhao, and C. S. Tian, Mater. Sci. Forum **546-549**, 2215 (2007).
[21] R. K. Bhuyan, T. S. Kumar, D. Goswami, A. R. James, and D. Pamu, J. Electroceram. **31** 48 (2013).
[22] C. L. Huang, M. H. Weng, C. C. Wu, and C. C. Wei, Jpn. J. Appl. Phy. **40**, 698 (2001).
[23] A. Y. Borisevich and P. K. Davies, J. Am. Ceram. Soc. **87**, 1047 (2004).
[24] Y. Wu and G. Cao, Appl. Phys. Lett. **75**, 2650 (1999).
[25] K. R. Kambale, S. Shroff, S. P. Butee, R. Singh, and A. R. Kulkarni, Ferroelectrics **518**, 94 (2017).
[26] I. T. Seo, H. Y. Park, N. V. Dung, M. K. Choi, S. Nahm, H. G. Lee, and B. H. Choi, IEEE Trans. Ultrason. Ferroelectr. Freq. Control. **56**, 2337 (2009).
[27] W. C. Tzou, C. F. Yang, Y. C. Chen, and P. S. Cheng, J. Eur. Ceram. Soc. **20**, 991 (2000).
[28] J. G. Fisher, H. Sun, Y. G. Kook, J. S. Kim, and P. G. Le, J. Magn. Magn. Mater. **416**, 384 (2016).
[29] R. Kohlmuller and J. Perraud, Bull. Soc. Chim. Fr. **3**, 642 (1964).
[30] A. C. F. M. Costa, E. Tortella, M. R. Morelli, and R. H. G. A. Kiminami, J. Magn. Magn. Mater. **256**, 174 (2003).
[31] Y. I. Jung, D. Y. Yoon, and S. J. L. Kang, J. Mater. Res. **24**, 2949 (2009).
[32] R. N. Bhowmik and A. Saravanan, J. Appl. Phys. **107**, 053916 (2010).
[33] R. D. Shannon, Acta Crystallographica Section A **32**, 751 (1976).